Laboratory Investigation (2013) 93, 733–743

Micro-computed tomography and nuclear magnetic resonance imaging for noninvasive, live-mouse cholangiography

James H Tabibian[1,2], Slobodan I Macura[3], Steven P O'Hara[1,2], Jeff L Fidler[4], James F Glockner[4], Naoki Takahashi[4], Val J Lowe[5], Bradley J Kemp[5], Prasanna K Mishra[3], Pamela S Tietz[1,2], Patrick L Splinter[1,2], Christy E Trussoni[1,2] and Nicholas F LaRusso[1,2]

The cholangiopathies are a diverse group of biliary tract disorders, many of which lack effective treatment. Murine models are an important tool for studying their pathogenesis, but existing noninvasive methods for assessing biliary disease *in vivo* are not optimal. Here we report our experience with using micro-computed tomography (microCT) and nuclear magnetic resonance (MR) imaging to develop a technique for live-mouse cholangiography. Using mdr2 knockout (mdr2KO, a model for primary sclerosing cholangitis (PSC)), bile duct-ligated (BDL), and normal mice, we performed *in vivo*: (1) microCT on a Siemens Inveon PET/CT scanner and (2) MR on a Bruker Avance 16.4 T spectrometer, using Turbo Rapid Acquisition with Relaxation Enhancement, IntraGate Fast Low Angle Shot, and Half-Fourier Acquisition Single-shot Turbo Spin Echo methods. Anesthesia was with 1.5–2.5% isoflurane. Scans were performed with and without contrast agents (iodipamide meglumine (microCT), gadoxetate disodium (MR)). Dissection and liver histology were performed for validation. With microCT, only the gallbladder and extrahepatic bile ducts were visualized despite attempts to optimize timing, route, and dose of contrast. With MR, the gallbladder, extra-, and intrahepatic bile ducts were well-visualized in mdr2KO mice; the cholangiographic appearance was similar to that of PSC (eg, multifocal strictures) and could be improved with contrast administration. In BDL mice, MR revealed cholangiographically distinct progressive dilation of the biliary tree without ductal irregularity. In normal mice, MR allowed visualization of the gallbladder and extrahepatic ducts, but only marginal visualization of the diminutive intrahepatic ducts. One mouse died during microCT and MR imaging, respectively. Both microCT and MR scans could be obtained in ≤ 20 min. We, therefore, demonstrate that MR cholangiography can be a useful tool for longitudinal studies of the biliary tree in live mice, whereas microCT yields suboptimal duct visualization despite requiring contrast administration. These findings support further development and application of MR cholangiography to the study of mouse models of PSC and other cholangiopathies.
Laboratory Investigation (2013) **93,** 733–743; doi:10.1038/labinvest.2013.52; published online 15 April 2013

KEYWORDS: animal models; biliary tract diseases; live-animal imaging; magnetic resonance cholangiopancreatography; primary sclerosing cholangitis; strictures

The cholangiopathies are an etiopathogenically diverse group of disorders affecting the epithelial cells that line the three dimensional (3D) tubular network of bile ducts.[1–5] Because of their prevalence, progression to liver cirrhosis and cancer, and largely obscure pathogenesis, cholangiopathies account for a substantial proportion of the morbidity and mortality of all liver diseases.[1,6,7] Critically important to unraveling the fundamental underpinnings of these complex disorders is the development of animal models and novel tools to better study and characterize them.[8,9]

Primary sclerosing cholangitis (PSC) is an example of a chronic, idiopathic cholangiopathy, which lacks effective medical therapy, and wherein animal models have begun to reveal mechanistic insights.[5,10,11] In the United States alone,

[1]Division of Gastroenterology and Hepatology, Mayo Clinic, Rochester, MN, USA; [2]Center for Cell Signaling in Gastroenterology, Mayo Clinic, Rochester, MN, USA; [3]Division of Biochemistry and Molecular Biology, Mayo Clinic, Rochester, MN, USA; [4]Division of Radiology, Mayo Clinic, Rochester, MN, USA and [5]Division of Nuclear Medicine, Mayo Clinic, Rochester, MN, USA
Correspondence: Dr NF LaRusso, MD, Division of Gastroenterology and Hepatology, Mayo Clinic, 200 First Street SW, Rochester, MN 55905, USA.
E-mail: larusso.nicholas@mayo.edu
Presented at the 63rd Annual Meeting of the American Association for the Study of Liver Diseases, Boston, MA, USA, 13 November 2012.

Received 12 December 2012; revised 19 February 2013; accepted 20 February 2013

the prevalence of PSC is estimated at 25 000 adolescents and adults, and estimated median survival from time of diagnosis to death or liver transplantation is 12 years.[6,7] PSC is characterized microscopically by biliary inflammation and fibrosis, and cholangiographically by biliary strictures alternating with dilatations and, hence, an irregular, 'ragged'-appearing biliary tree.[10,12–14] Currently, the most widely used model of PSC is the mdr2 (abcb4) knockout (mdr2KO) mouse.[8,9] Biliary disease in this model is due to increased hydrophobicity of bile (as a result of decreased phospholipid content), and includes cholesterol gallstones, multifocal biliary strictures and dilations, cholestasis, and biliary fibrosis.[8,12,15] Aside from serum biochemical data, assessment of biliary disease in the mdr2KO mouse, as well as alternative murine models of PSC and other cholangiopathies, relies heavily on liver histology; this, however, requires killing the animal and limits longitudinal monitoring and is resource consuming.

Noninvasive imaging continues to gain importance and use in both clinical management and animal models of the cholangiopathies and other diseases. Since its initial description over 20 years ago,[16] noninvasive hepatobiliary imaging with magnetic resonance (MR) cholangiopancreatography (MRCP) has evolved into an important modality for the diagnosis and longitudinal surveillance of PSC and other cholangiopathies.[13,17,18] MRCP provides valuable, global anatomic data regarding hepatobiliary disease. However, it has some inherent limitations; eg, motion artifacts can lead to suboptimal image quality and cause false-positive interpretations or poor visualization of the bile ducts. In addition, the spatial resolution of MR may not allow visualization of small intrahepatic bile ducts. Because of these limitations, some investigators have evaluated computed tomography (CT) cholangiography. CT cholangiography offers various theoretical advantages that can allow better visualization of smaller ducts but requires the administration of a contrast agent that is excreted into the biliary system.[19–21] These contrast agents, however, increase the risks associated with the exam and may not be excreted well in livers with impaired function, thus leading to poor visualization of the bile ducts. In mouse models of cholangiopathy, a noninvasive hepatobiliary imaging method is needed but is currently lacking.

There are several major challenges associated with live-mouse abdominal imaging, particularly cholangiography. These include the simultaneous need for high resolution (due to the diminutive size of murine bile ducts), high speed (to eliminate motion artifact from the lungs, heart, bowel, and biliary smooth muscle), high contrast (to distinguish bile ducts from surrounding liver tissue and adjacent blood vessels), and short duration of scans (to not cause undue morbidity). Thus, the purpose of this study was to investigate the methodological feasibility of micro-computed tomography (microCT) and MR imaging for noninvasive, live-mouse cholangiography and evaluate their potential utility in assessing mouse models of cholangiopathy *in vivo*.

MATERIALS AND METHODS

Experimental Animals

All animal procedures were reviewed and approved by, and conducted in accordance with, the Mayo Clinic Institutional Animal Care and Use Committee. A total of 15 mdr2KO (9 female, 6 male) mice, 7 wild-type (WT) mice (4 female, 3 male), and two bile duct-ligated (BDL) mice (1 female, 1 male) were included in this study. WT mice were used as negative controls. BDL mice were used as positive controls to assess the ability of imaging to differentiate between acute biliary obstruction and sclerosing cholangitis (ie, mdr2KO mice); one BDL mouse underwent common bile duct (CBD) ligation, while the other underwent selective right hepatic duct ligation. All mice were between 4 and 8 months of age and weighed a median of 22 g (range 19–29).

Mdr2KO mice were killed and dissected immediately after imaging to correlate imaging results with intraoperative findings. For mdr2KO mice that did not have grossly distinguishable (ie, uniquely characteristic) biliary tract features, livers were perfused with 10% neutral buffered formalin, and liver histopathology was assessed with Masson's Trichrome-stained paraffin-embedded serial sections as previously described[22] to corroborate imaging findings. Similarly, one BDL mouse was killed and dissected immediately after imaging and was examined grossly and histopathologically.

Mice were bred and maintained at the animal facility at Mayo Clinic, with a 12 h light/dark cycle and free access to standard mouse chow and water.

Mouse Preparation and Imaging

Mice were fasted for up to 6 h before imaging. Anesthesia was induced in an animal chamber with a gas mixture of oxygen (1 l/min) and 2% isoflurane (Abbott Laboratories, North Chicago, IL, USA). Following anesthesia, mice were transferred to a small rodent cradle or mouse coil for microCT and MR imaging, respectively. Anesthesia was maintained with 1.5–2.5% inhalational isoflurane.

Micro-computed tomography

MicroCT was performed using a Siemens Inveon PET/CT scanner (Siemens Medical Solutions, Knoxville, TN, USA). Parameters were as follows: 360° rotation, 360 projections, 500 ms exposure time, 80 kV voltage, 500 μA current, and effective pixel size 28.09 μm. Acquisitions were reconstructed with a filtered backprojection algorithm, matrix size $512 \times 512 \times 256$, using manufacturer-provided software.

To allow visualization of the biliary tree, three mice were injected intraperitoneally (IP) and two mice were injected intravenously (IV) with iodipamide meglumine (Cholografin) biliary contrast (Bracco Diagnostics, Princeton, NJ, USA). Escalating doses from 0.9 to 3 ml/kg were used based on body surface area normalization and results of preliminary scans.[23] IP injection was performed in the left lower quadrant of the abdomen post-induction of anesthesia.

IV injection was performed in the tail vein with mice in a custom cylindrical restrainer and under a heat lamp pre-induction of anesthesia. Mice were scanned at multiple time points after contrast injection.

Each mouse was scanned for up to a total of 2 h per day to evaluate different scans (eg, with and without contrast at different time points post-contrast administration). Scans lasted $\sim$11 min. After scanning, mice were observed for 1 h to ensure adequate reheating and anesthetic recovery.

Magnetic resonance

MR imaging was performed using a Bruker Avance 700 MHz, 16.4 T vertical bore MR spectrometer equipped with mini-imaging accessories (Bruker BioSpin, Billerica, MA, USA). A 16.4 T spectrometer was used to maximize sensitivity (ie, signal-to-noise ratio, SNR). As a result of shortening of the T2 (and T2*) and lengthening of the T1 tissue water relaxation times at such high field strengths, repetition time (TR) must be longer and echo time (TE) shorter at 16.4 T than at 7 T in order to maintain the same detectable magnetization. The most notable effect of the T2 shortening is that the RARE factor must be lower. Thus, although imaging at 16.4 T results in SNR improvements, these are partially offset by the changes in relaxation time change, the end outcome of which is better images at higher fields, albeit less so than expected.

In addition to the aforementioned challenges associated with mouse cholangiography, there are several others which are generally not an issue in clinical MRCP; eg, the mouse heart is located much closer to the liver, beats nearly an order of magnitude faster, and causes oscillatory motion that is on the magnitude of mouse bile duct size. Therefore, we evaluated several different measuring (ie, imaging) methods, each with a varying range of acquisition parameters, to determine which would provide the best visualization of the biliary tree, particularly the intrahepatic bile ducts (Table 1). The three methods that we ultimately pursued based on promising initial results were Turbo Rapid Acquisition with Relaxation Enhancement (TurboRARE), Half-Fourier Acquisition Single-shot Turbo Spin Echo (HASTE), and IntraGate Fast Low Angle Shot (IntraGateFLASH). As described below, each of these three methods has certain properties (or is compatible with additional manipulations) that mitigate motional artifacts or offer other advantages.

TurboRARE, a spin echo technique, was the primary 3D method investigated. TurboRARE imaging was performed in conjunction with respiratory triggering or gating to eliminate respiratory motion artifact; this is important as images are obtained by Fourier transformation of the true 3D raw data from k-space, and motion anywhere in the field of view (FOV) during a scan produces artifact along phase and slice domains. To reduce the fraction of blanking time with respiratory gating, the respiratory rate was continuously monitored (SA Instruments, New York, NY, USA) and controlled by adjusting the heating air temperature (34–37 °C) and isoflurane concentration (1.5–2.5%). Normally, in 3D methods the FOV must cover the whole visible object to avoid aliasing. As normal intrahepatic bile ducts have a diameter on the order of 100 μm, in-plane resolution of approximately the same size is required. With FOV 51.2 mm $\times$ 25.6 mm $\times$ 25.6 mm, a matrix of 512 $\times$ 256 $\times$ 256 is necessary, meaning that 65 000 (256^2) k-space vectors need to be acquired for a 3D data set with 100 μm/voxel isotropic resolution. Thus, for high-resolution images (where 10 000–65 000 k-space vectors need to be collected), 3D methods are intrinsically time-intensive, and even more so when combined with respiratory triggering (and to a lesser extent gating) techniques. Contributing to this long scanning time is the aforementioned principle of tissue water T2 (and T2*) relaxation time becoming shorter and T1 becoming longer at

Table 1 Summary of MR cholangiography methods and parameters

	Parameters				
Methods	Repetition time, ms	Echo time, ms	Resolution, μm/pixel	Slice thickness, mm	Acquisition time, mins
Without gadoxetate disodium					
IntraGateFLASH	25–200	1.2–5	100–150 in-plane	0.25–1	4–34
HASTE	245–3000	1.2–4.2	200–250 in-plane	0.2–0.5	3–18
TurboRARE	NA (respiratory triggered)	30–43 (effective)	100–200 isotropic	NA (3D)	34–60
With gadoxetate disodium					
TurboRARE	150 (respiratory gated)	16 (effective)	100–200 isotropic	NA (3D)	19–25

IntraGateFLASH, IntraGate Fast Low Angle Shot; HASTE, Half-Fourier Acquisition Single-shot Turbo Spin Echo; TurboRARE, Turbo Rapid Acquisition with Relaxation Enhancement.
Methods and parameters, which yielded favorable imaging results are provided. Two other methods were also investigated, Fast Imaging with Steady State Precession (FISP) and Echo planar imaging (EPI), but were not found to be useful for mouse cholangiography. Additional details are provided in the figure legends.

higher fields, as a result of which RARE factor is restricted to ≤ 16 and TR to > 1000 ms. Therefore, despite the strengths of TurboRARE methodology, there is an associated time penalty.

IntraGateFLASH, a gradient echo technique, eliminates periodic motional artifacts by recording the scout scan before each k-space vector and by reconstructing images from the k-space vectors with similar scout scans (a form of retrospective gating). Thus, acquisition must be repeated many times (10–100) to create a vector library large enough to have a number of k-space vectors with the same scout phase to generate essentially artifact-free images. Performing more repetitions helps eliminate respiratory and cardiac artifact, but also leads to longer scan time. The number of repetitions needed is largely dependent on and increases with the amount of motion (eg, respiratory) and may range from 10–15 repetitions (yielding an approximate scan time of 5–10 min) to 50–100 repetitions (yielding an approximate scan time of 20–30 min). Of note, although clinically used FLASH (ie, for MRCP) is T1 weighted, we lengthened the echo time to include T2* weighting.

HASTE, an ultrafast spin echo technique, eliminates motional artifacts by rapidly collecting data from a single slice. Although respiratory motion artifact is not difficult to eliminate, cardiac motion artifact is challenging. Depending on the body temperature and degree of anesthesia, the mouse heart rate ranges between 250–500 beats/min, with a motional period between 150–240 ms. Thus, acquisition times should ideally be shorter than 100 ms. With an estimated echo time of 4 ms (based on anticipated resolution and spectral width), this 100 ms threshold is reached with RARE factor 20–30. To maintain resolution on the order of 200 μm/pixel, a single slice is generated in two to four segments; with repetition times on the order of seconds, this can be acquired within a few seconds. The biliary tree can then be reconstructed from multislice data; thus, 20 to 200 thin slices are collected, resulting in a total acquisition time of 3–20 min. In addition to acquisition being faster than the heartbeat, the main advantage of HASTE in comparison with TurboRARE is that it is inherently a 2D method; thus, motional artifacts (if any) do not propagate between the slices. Therefore, even if some slices are corrupted, a useful image of the biliary tree can still be obtained.

In addition to the above techniques, we also evaluated the utility of IP gadoxetate disodium (Eovist, Bayer, Berkeley, CA, USA), a gadolinium-containing paramagnetic contrast agent that is excreted through the biliary system, for improving duct visualization. The dose used was based on the body surface area normalization method.[23] We also assessed the utility of using IP glucagon (Sigma-Aldrich, St Louis, MO, USA) at a dose of 0.15 mg/kg to help decrease gut motion artifact.[24] Both gadoxetate disodium and glucagon were injected in the left lower quadrant of the abdomen immediately before scanning.

MR scan times ranged from $\sim$2–70 min, depending on the method and parameters used. Mice were imaged for up to a total of 4 h per day and observed for 1 h afterward to ensure anesthetic recovery.

Image Processing and Analysis

PMOD Biomedical Image Quantification and Kinetic Modeling Software version 2.85 (PMOD Technologies, Zurich, Switzerland) and Paravision 5.0/5.1 software (Bruker BioSpin) were used to process and inspect microCT and MR images, respectively. MR images were also post-processed by using a maximum-intensity projection (MIP) algorithm to create a projection cholangiogram that could be rotated and viewed from user-defined angles.

Visualization of the following biliary structures in mdr2KO mice, BDL mice, and control mice was assessed by at least three coinvestigators experienced in hepatobiliary imaging: gallbladder, extrahepatic (including hilar) bile ducts, and intrahepatic bile ducts. In addition, detection of (1) cholelithiasis, ductal dilation, strictures, and irregularity was assessed in mdr2KO mice, and (2) gallbladder and ductal dilation was assessed in BDL mice.

Ductal dilation was defined as any duct with a diameter > 300 μm or any intrahepatic duct with a diameter > 150 μm or beyond third order (ie, branching).[25] Ductal stricture was defined as a focal (circumferential) luminal narrowing or tapering with upstream dilation.[26] Ductal irregularity was defined as either strictures alternating with normal or dilated-appearing ducts or as 'ragged'-appearing intrahepatic ducts, as seen in PSC.[13,27,28]

RESULTS

Micro-computed Tomography

MicroCT scans were performed in three mdr2KO mice (two female, one male). Preliminary scans without biliary contrast injection resulted in nonvisualization of biliary structures due to inadequate hepatic soft tissue contrast. Therefore, mice were rescanned after IP injection of iodipamide meglumine biliary contrast. This modification yielded visualization of the gallbladder, extrahepatic ducts, and intrahepatic ducts in three, two, and none of the three mdr2KO mice, respectively (Figure 1a). It was noted that hyperdense intragastric chow appeared to obscure images by causing streaking artifact, and thus fasting periods of 4 h were made standard. This modification resulted in reduced artifact, but again, intrahepatic ducts could not be identified.

Therefore, subsequent microCT imaging was performed with IV biliary contrast administration in addition to 6 h fasting. This yielded marginally improved visualization of hilar ducts, but intrahepatic ducts (or any features of sclerosing cholangitis) again could not be definitively identified (Figure 1b), regardless of the time interval between contrast administration and imaging. Of note, peak biliary excretion following intravenous contrast occurred after $\sim$15 min. Despite higher concentrations of IV contrast, the only appreciable change was the greater amount of contrast in the proximal small bowel (unintentionally yielding

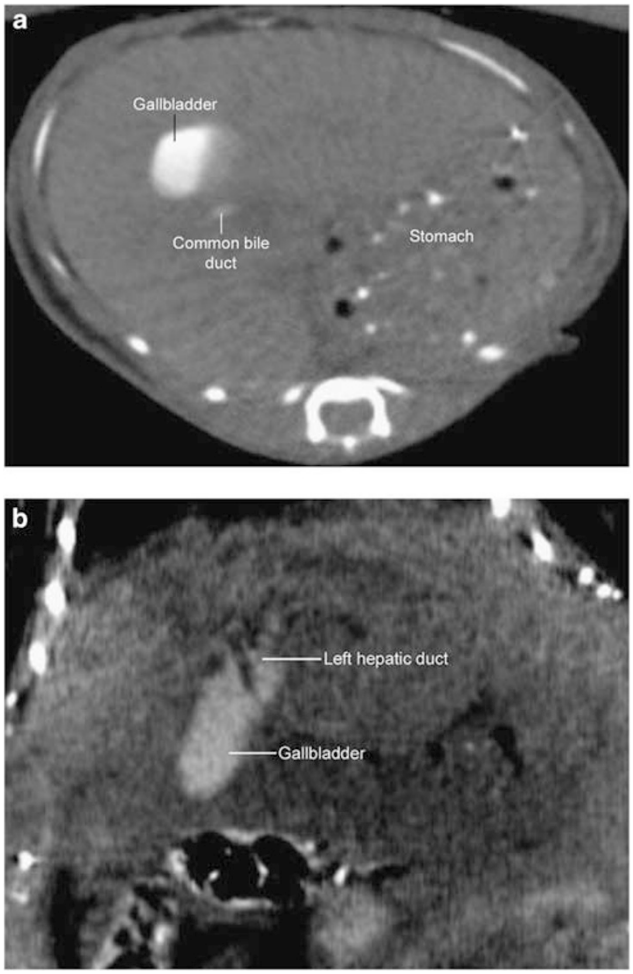

Figure 1 Contrast-enhanced micro-computed tomography (microCT) image of mdr2 knockout (mdr2KO) mouse. (**a**) Intraperitoneal contrast-enhanced axial image demonstrating a normal-appearing gallbladder and common bile duct; intrahepatic ducts are not visualized. Hyperdense gastric contents are present and cause streak artifact. (**b**) Intravenous contrast-enhanced coronal image demonstrating normal-appearing gallbladder and dilated hilar ducts; intrahepatic ducts are again not visualized despite addition of 6 h fasting.

enterographic images). In addition, one mouse that received a dose of 3 ml/kg of IV contrast in a single session died within a day. The other two mdr2KO mice survived IP and IV contrast injection, microCT scanning, and anesthesia.

Because of the need for invasive contrast injection, the mortality associated with higher doses of contrast, and the nonvisualization of intrahepatic ducts despite these maneuvers, further investigation with microCT was not pursued. These results, and those from MR imaging, are summarized in Table 2.

Magnetic Resonance

mdr2KO mice

Preliminary MR imaging was performed with the same three mdr2KO mice used for microCT. Using a variety of mostly T2-weighted methods, there was good contrast between the biliary tree and surrounding liver tissue; this was achieved without administration of contrast and facilitated by the long T2 relaxation time of bile. The gallbladder and extrahepatic ducts were readily visualized in all three mdr2KO mice, and intrahepatic ducts were visualized in two of the three mice. Cholelithiasis was noted in these same two mice as round, hypointense filling defects (Figure 2a). One of these mice also had a markedly dilated CBD (1 mm in diameter) with choledocholithiasis, which was confirmed by anatomic dissection immediately after imaging (Figure 2b).

Notably, it became apparent that scans longer than 20–25 min generally resulted in compromised image quality. This time penalty was likely related to spontaneous biliary smooth muscle contraction, varying respiratory and heart rates, periodic respiratory 'sighs' (ie, high-amplitude breaths), and intestinal motion. Although nonrespiratory-gated, rapid imaging could adjust for some of these factors with image oversampling and retrospective gating (ie, IntraGateFLASH method), it was not compatible with 3D imaging (but was useful for high resolution (eg, 100 μm) in-plane images). Glucagon administration to reduce intestinal motion had no apparent effect on image quality (data not shown).

Five additional mdr2KO mice were scanned in an attempt to modify methodology and improve visualization of intrahepatic ducts. Using 3D respiratory-triggered TurboRARE, intrahepatic ducts were more clearly visualized, and MIP post-processing algorithms yielded visualization of the intrahepatic biliary tree in its totality, revealing irregular, strictured, dilated intrahepatic ducts consistent with sclerosing cholangitis (Figure 3a). Additional morphological details could be seen by rotating the 3D MIP video files, including 'beading' of the intrahepatic ducts in some mice, a feature characteristic of PSC (Figure 3b and Supplementary Video S1). Liver histology in these mice confirmed sclerosing cholangitis (Figure 3c), thus accounting for and corroborating the cholangiographic appearance. Notably, ductal abnormalities on MR imaging appeared more prominent in female mice; this discrepancy is consistent with the prior observation that hepatic biochemical parameters are more deranged in female as compared with male mdr2KO mice.[29] All mdr2KO mice survived anesthesia and MR imaging.

WT (negative control) mice

Seven WT mice were imaged with the same methods as above. Although the gallbladder and (at least a portion of) extrahepatic ducts were consistently visualized, visualization of the intrahepatic ducts was generally marginal despite satisfactory contrast and suppression of vascular structures, such as portal veins (Figure 4), albeit improved with 2D respiration-triggered HASTE imaging. When visualized, ducts were diminutive (none $>300\,\mu$m), fewer in number compared with mdr2KO mice, and smooth, ie, without appreciable abnormalities. Glucagon administration pre-imaging did not appreciably improve image quality or

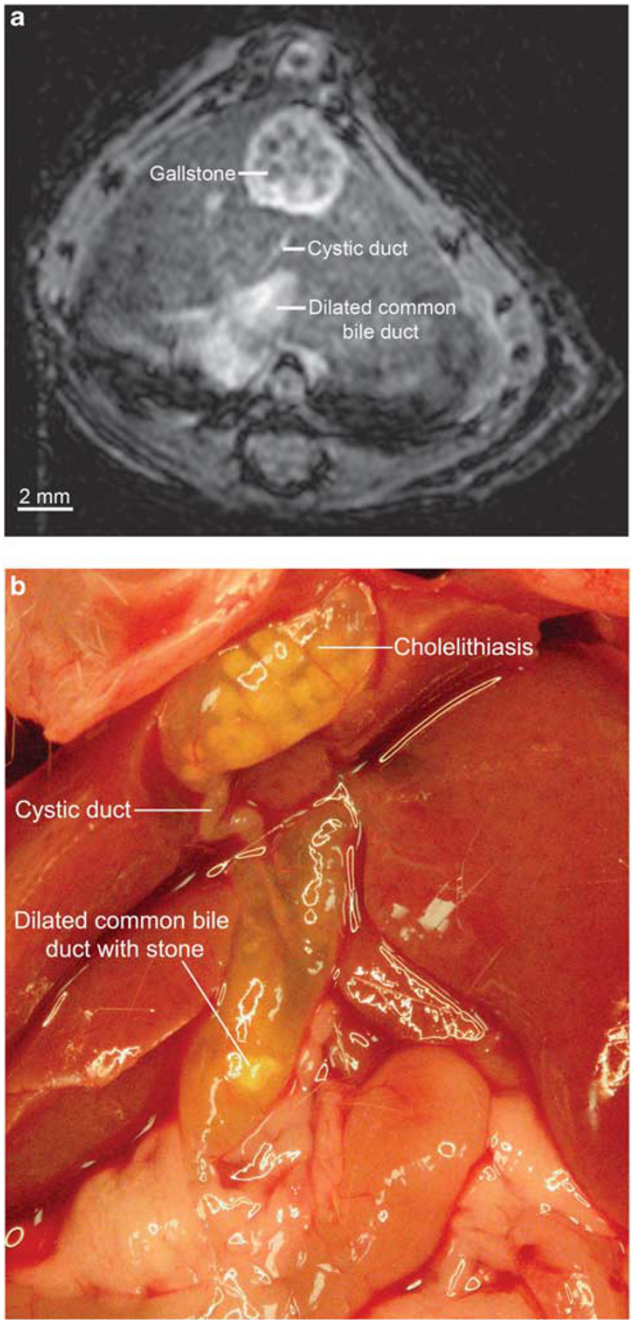

Figure 2 Cholelithiasis and dilated common bile duct in mdr2 knockout (mdr2KO) mouse seen with magnetic resonance (MR) imaging and confirmed by anatomic dissection. (**a**) Gallstones are seen as 0.35 mm, circular hypointensities. Common bile duct is dilated to over 1 mm, whereas the cystic duct appears to be of normal or slightly enlarged caliber (IntraGateFLASH (IntraGate Fast Low Angle Shot), echo time 3 ms, repetition time 82 ms, 30 repetitions, image matrix 256 × 256 pixels, acquisition matrix size 128 × 128 pixels, resolution 125 × 125 μm, slice thickness 250 μm, acquisition time 5.3 min). (**b**) Dissection of the same mouse immediately after imaging demonstrates extensive cholelithiasis and a severely dilated common bile duct with choledocholithiasis, consistent with MR findings.

visualization of ducts. All WT mice survived anesthesia and MR imaging.

BDL mice

BDL mice were used to interrogate the ability of MR imaging to differentiate between acute biliary obstruction and the sclerosing biliary disease seen in mdr2KO mice. BDL mice were imaged 1 and 2 days post-BDL, during which time progressive biliary tree dilation was visualized. By the second day, the mouse with CBD ligation was found to have a markedly dilated gallbladder with a distinct, round morphology (Figure 5a). The mouse with selective right hepatic duct ligation demonstrated increasing ductal dilation and hyperintensity of the right side of the liver (Figure 5b). This mouse was dissected after the second day, and corresponding findings of a right liver lobe infarction were observed grossly (Figure 5c) and on histopathology (Supplementary Figure S1).

The overall condition of both BDL mice was tenuous, and maintaining stable vital signs was difficult. Fortuitously, however, it became apparent that after ~1 h of anesthesia and acclimation of the mouse inside the MR spectrometer, respiratory (and heart) rate became more regular and could be stably suppressed and maintained at 20–30 breaths/min. During this 'deep' anesthesia, for reasons that are discussed later, longer imaging times (up to 60 min) were possible and yielded superior 3D imaging results (Figure 5d and Supplementary Video S2). As can be seen, although the gallbladder and bile ducts were diffusely dilated in the BDL mice, there was no evidence of ductal strictures or irregularity, thus allowing accurate distinction between BDL and mdr2KO mice.

Both BDL mice survived anesthesia and MR imaging, but were killed after day 2 of imaging.

Gadoxetate disodium contrast-enhanced imaging of mdr2KO mice

Although the biliary tree was generally well-visualized with MR in diseased mice without contrast administration, we explored the incremental utility of IP contrast enhancement in seven additional mdr2KO mice. We found that at parameters optimized for contrast-enhanced imaging, use of gadoxetate disodium allowed for improved visualization of the biliary tree, particularly the intrahepatic ducts (Figure 6a). Specifically, it increased SNR and mitigated the time penalty needed for high-resolution scanning. This is further demonstrated in Figure 6b (and Supplementary Video S3), wherein 100 μm isotropic resolution 3D cholangiography could be obtained in only 25 min (as compared with 45–60 min without contrast). Of note, one mouse died following contrast administration.

DISCUSSION

In this study, we investigated the feasibility and utility of using noninvasive imaging to perform live-mouse

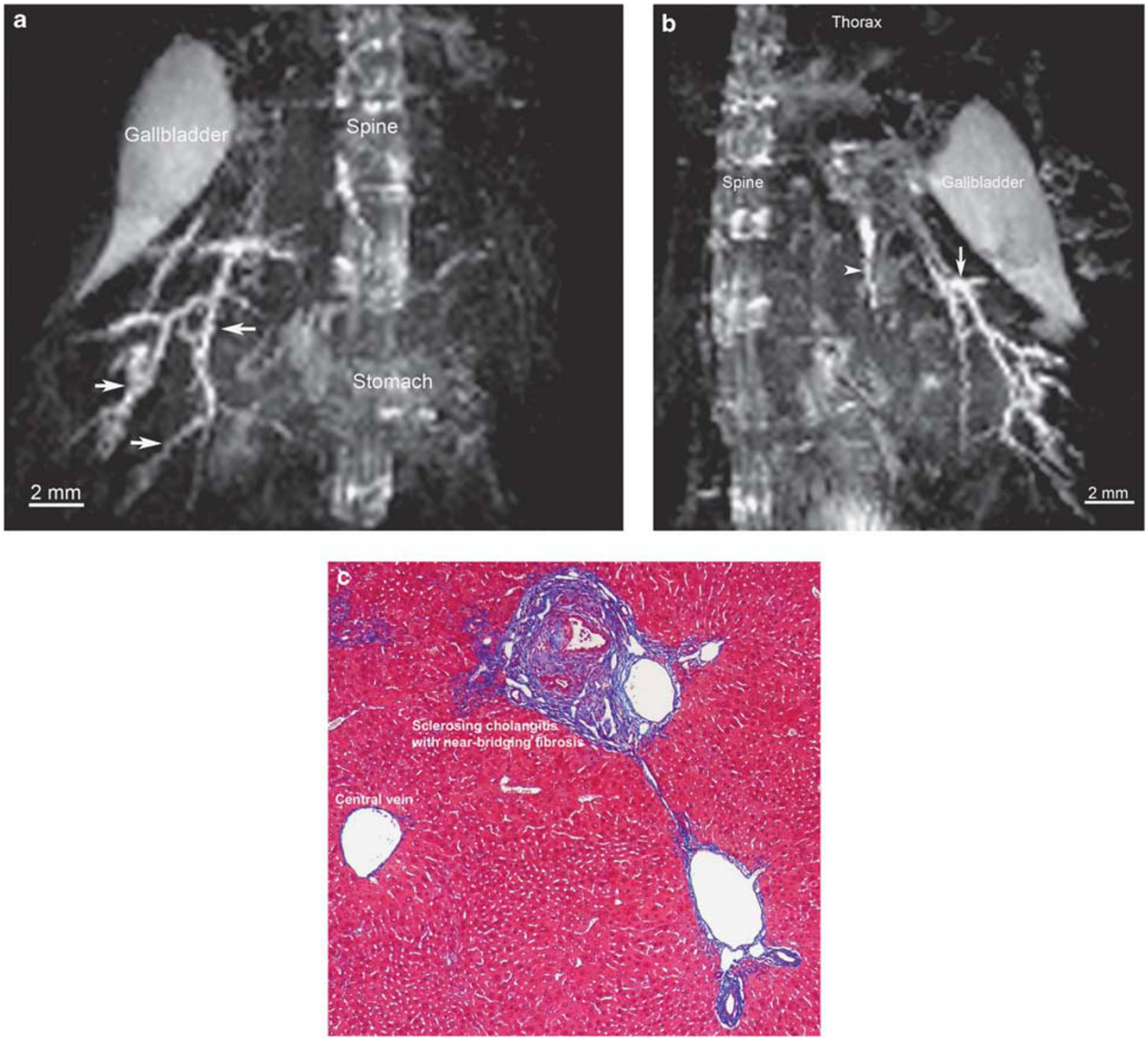

Figure 3 Magnetic resonance (MR) imaging with maximum intensity projection (MIP) post-processing demonstrates intrahepatic changes consistent with sclerosing cholangitis in mdr2 knockout (mdr2KO) mouse, as corroborated by liver histology. (**a**) Coronal view of mdr2KO mouse biliary tree using MIP algorithm demonstrates dilated, diffusely irregular intrahepatic ducts (arrows) (TurboRARE (Turbo Rapid Acquisition with Relaxation Enhancement) with respiratory triggering, echo time 8 ms, effective echo time 24, RARE factor 8, image and acquisition matrix $256 \times 128 \times 128$ pixels, resolution 200 μm isotropic, acquisition time 39 min with respiratory rate of $\sim$70 breath/min). (**b**) On sagittal view, the same MIP demonstrates additional features, including beading (arrow) and a sclerotic left ductal system, hallmarks of primary sclerosing cholangitis. (**c**) Trichrome-stained section of mdr2KO mouse liver ($\times$10) demonstrates characteristic features of sclerosing cholangitis, consistent with MR findings.

cholangiography. Our work demonstrates that: (1) microCT yields suboptimal bile duct visualization despite escalating doses of IP and IV contrast; (2) MR is safe and allows visualization of the gallbladder, extra-, and intrahepatic bile ducts in nearly all mdr2KO mice without requiring contrast administration; (3) the cholangiographic appearance of mdr2KO mice is similar to human PSC; (4) MR cholangiography can differentiate between mdr2KO, BDL, and WT mice; and (5) use of gadoxetate disodium MR contrast can improve duct visualization and shorten scan times. To our knowledge, this is the first study of noninvasive, live-mouse cholangiography; the findings herein suggest that MR cholangiography is a promising novel modality to non-invasively and longitudinally examine mouse (and likely other small rodent) models of PSC and other cholangiopathies, including polycystic kidney and liver disease,[30] *C. parvum*-induced cholangitis,[31] and hepatic graft *versus* host disease.[32] As such, it holds potential as a new tool to better study disease pathogenesis and therapeutic response in existing models of cholangiopathy and facilitate development

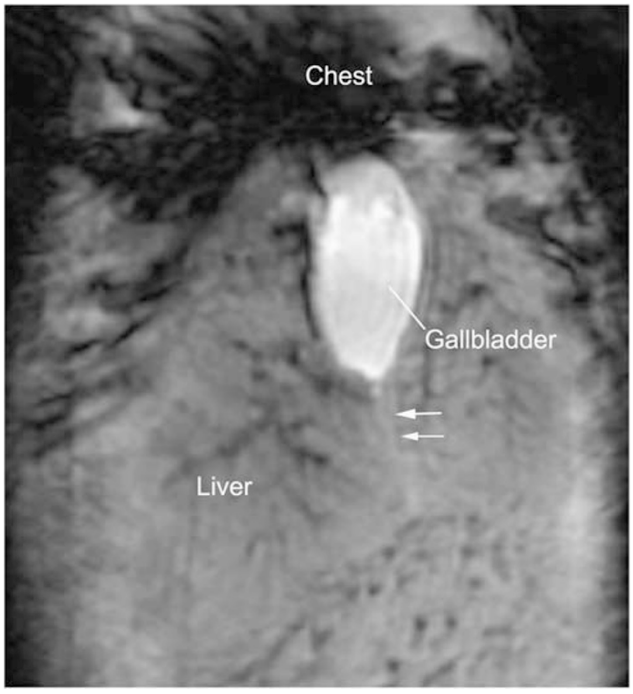

Figure 4 Coronal magnetic resonance (MR) image of wild-type mouse demonstrating normal-appearing gallbladder and a faint linear hyperintensity (white arrows) suggestive of the cystic duct. Black streaks in the liver represent attenuated vascular structures (IntraGateFLASH (IntraGate Fast Low Angle Shot), echo time 4 ms, repetition time 200 ms, 80 repetitions, image matrix 512×256 pixels, acquisition matrix size 256×128 pixels, resolution $100 \times 100\,\mu$m, slice thickness 1 mm, acquisition time 34 min).

of novel and more clinically relevant models. In addition, MR cholangiography may accelerate translation of animal model findings to the clinical arena, wherein MRCP has not only enhanced patient care, but is also emerging as an endpoint in clinical trials.

Drawing on our experience with MRCP and based on results obtained herein from our mouse imaging experiments, several important observations were made in this study. Fasting of mice was noted to be an important prerequisite as with hepatobiliary imaging in humans; the mechanism involved is not entirely clear, but is likely a combination of increased bile-duct filling and decreased smooth muscle activity in bile ducts and viscera. Glucagon administration had no apparent effect on image quality; opioid agonists such as morphine could be more effective in this regard and may merit future exploration, although with caution to not cause undue mouse morbidity. Respiratory triggering or gating was imperative in certain methods (ie, 3D TurboRARE), but was less critical with faster imaging (ie, HASTE) and image oversampling (ie, IntraGateFLASH) methods. Moreover, the utility of respiratory triggering or gating was compromised when mouse respiratory rate was irregular or rapid; this said, as mentioned previously, we observed that deep anesthesia (ie, after 1 h of mouse acclimation to being inside the spectrometer and under anesthesia) permitted mouse stabilization and longer scans without SNR diminution due to artifact, thus yielding superior image quality (Figure 5d and Supplementary Video S2). Lastly, as with clinical MRCP, there are certain strengths and weaknesses to each imaging method; eg, we found that 2D HASTE and IntraGateFLASH yielded rapid scans with excellent in-plane resolution, whereas 3D TurboRARE with post-processing using a MIP algorithm provided a simplified, highly useful global view of the biliary tree in a single image (or video). Another advantage of HASTE is that motion artifact is localized within the affected slice (ie, it does not propagate through the whole image).

Although mouse abdominal imaging with microCT and MR is well established, the application of these techniques to performing dedicated live-mouse cholangiography has not been described until now. It should be noted, though, that other methods of studying the murine biliary tree have been reported. For example, near-infrared fluorescent cholangiography has been recently applied to murine biliary imaging; although preliminary results appear favorable, this is an intraoperative technique that requires laparotomy and intravenous injection of a fluorochrome probe.[33] In addition, even in the setting of complete biliary obstruction, it has not been shown to allow visualization of intrahepatic ducts, whereas this was achieved with our methods (Figures 5a and d, and Supplementary Video S2). We and others have shown that biliary casting provides excellent information regarding biliary architecture, but this is a labor-intensive technique that requires killing the animal and *ex vivo* retrograde biliary injection of liquid resin, thus precluding longitudinal studies.[34,35] Diffraction-enhanced radiography has been previously reported, but this too is performed *ex vivo* and does not differentiate well between bile ducts and veins, particularly in non-BDL mice.[36] Therefore, although a number of alternative methods exist, they are substantially more invasive, labor-intensive, and/or less sensitive than those that we have described herein.

Several limitations merit acknowledgment in our study. For microCT, we did not employ nanoparticulate contrast, continuous infusion of contrast through an IV catheter, respiratory triggering or gating, or deep anesthesia (ie, for $\geq$1 h before imaging); although these maneuvers would more fully interrogate the potential of microCT, we believe they would result in only modest improvements. In addition, they would not alter the fact that microCT mandates contrast administration to visualize the biliary tree and would likely lead to increased labor and/or costs. With respect to MR, our preliminary experiments on 7-T spectrometers suggest that longer echo times could be used, but this gain does not fully compensate for the superior sensitivity of the 16.4 T system; imaging with 3 T clinical scanners does not provide adequate resolution to visualize the murine biliary tree (data not shown). Slice thickness was not a focus of

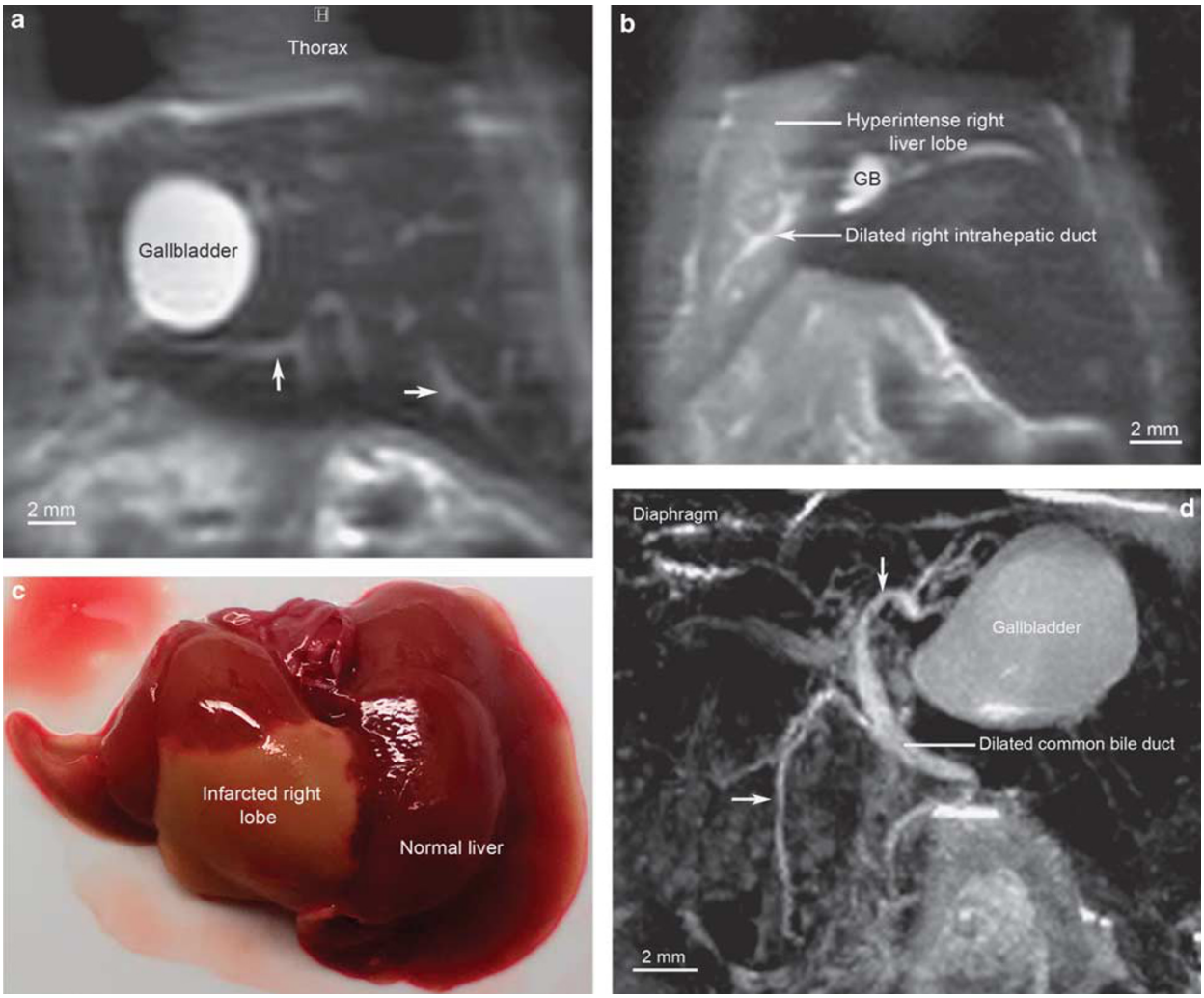

Figure 5 Images of bile duct-ligated mice demonstrating dilated biliary tree (without sclerotic changes) and bile infarct. (**a**) Coronal magnetic resonance (MR) image of common bile duct (CBD)-ligated wild-type mouse wherein gallbladder (GB) is dilated to 5 mm in largest dimension, and multiple intrahepatic ducts (arrows) are seen as a result of biliary obstruction (HASTE (Half-Fourier Acquisition Single-shot Turbo Spin Echo), echo time 3.9 ms, effective echo time 19.5 ms, repetition time 3000 ms, 4 repetitions, RARE factor 36, image matrix 256×128 pixels, acquisition matrix size 256×72 pixels, resolution $250 \times 250\ \mu$m, slice thickness 0.5 mm, acquisition time 24 s per slice). (**b**) Coronal MR image of right hepatic duct-ligated mouse demonstrating dilated right ductal system and right liver lobe hyperintensity, suggesting infarction (HASTE, echo time 4.18 ms, effective echo time 20.9 ms, repetition time 3000 ms, 4 repetitions, RARE factor 36, image matrix 256×128 pixels, acquisition matrix size 256×72 pixels, resolution $250 \times 250\ \mu$m, slice thickness 0.5 mm, acquisition time 24 s per slice). (**c**) Dissection immediately after MR imaging on day 2 post-right hepatic duct ligation revealing gross findings of right liver lobe infarction *ex vivo*, corroborating *in vivo* MR findings. (**d**) Sagittal view of CBD-ligated mouse biliary tree using maximum intensity projection post-processing algorithm demonstrating massively dilated GB, extra-, and intrahepatic ducts (arrows) (TurboRARE (Turbo Rapid Acquisition with Relaxation Enhancement) with respiratory gating, echo time 8.45 ms, effective echo time 42.2, RARE factor 16, image matrix $512 \times 256 \times 200$ pixels, acquisition matrix $364 \times 176 \times 142$ pixels, resolution 100 μm isotropic, acquisition time 59 min with respiratory rate of $\approx$25 breath/min).

this study, although in general, increasing slice thickness resulted in higher SNRs, albeit sacrificing anatomic details. We did not systematically remove nonhepatobiliary structures, such as spine or stomach, from MIP images and videos; in future studies, we hope to crop these structures pre-projection so as to maximize contrast and image clarity and facilitate quantitative measurements. Lastly, the number of animals investigated was limited, but adequate to complete the objectives of this preliminary study.

The experiences herein have led to valuable insights for further improvement and protocol development, including the following suggestions: (a) fasting mice for $\sim$6 h before imaging; (b) pre-anesthetizing for at least 1 h before imaging; (c) maintaining respirations at 20–30 breaths/min, particularly for respiratory-gated TurboRARE scans; (d) respiratory gating or multiple repetitions (ie, oversampling) to adjust for respiratory motion; and (e) considering use of gadoxetate disodium MR contrast to enhance duct visualization and

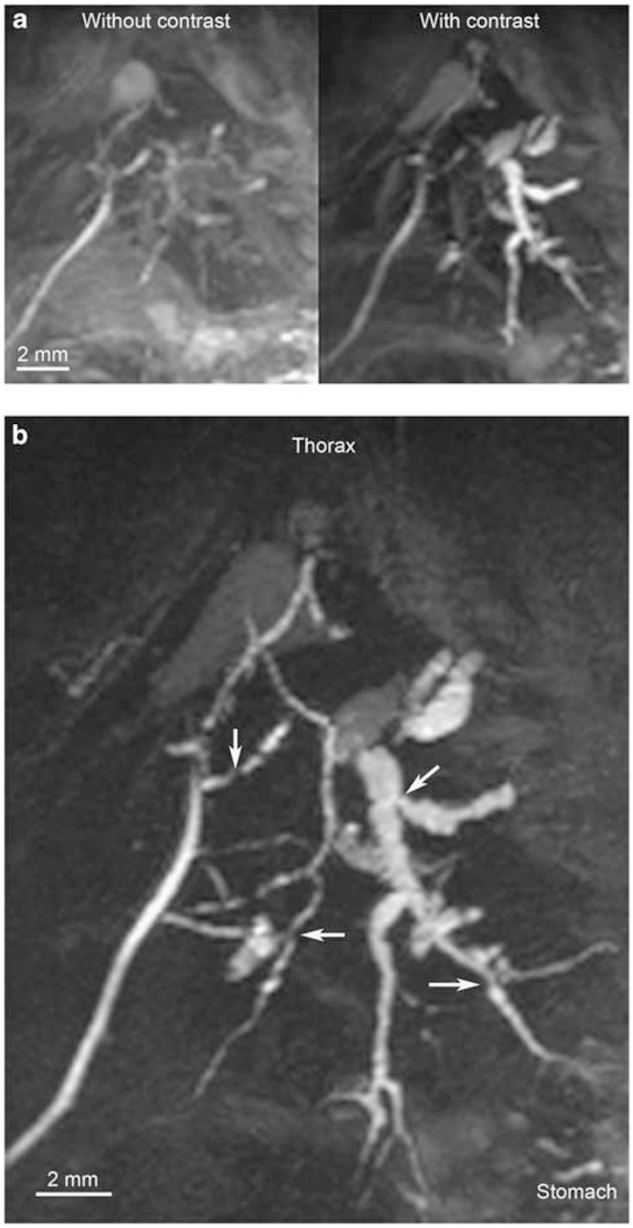

Figure 6 Maximum intensity projection (MIP) magnetic resonance (MR) images of mdr2 knockout (mdr2KO) mice with and without contrast. (**a**) With acquisition parameters optimized for contrast use (including shorter scan times, which would not be achievable without contrast), use of gadoxetate disodium (right) allows improved visualization of the biliary tree, particularly the intrahepatic ducts (TurboRARE (Turbo Rapid Acquisition with Relaxation Enhancement) with respiratory gating (TR 500) and partial Fourier transform acceleration factor 1.3, echo time 8 ms, effective echo time 16, RARE factor 4, image matrix $256 \times 128 \times 128$ pixels, acquisition matrix $197 \times 84 \times 100$ pixels, resolution 200 μm isotropic, acquisition time 19 min for each scan with respiratory rate of $\approx$25 breath/min). (**b**) Accelerated, high-resolution *in vivo* cholangiography facilitated by gadoxetate disodium-enhancement demonstrating irregular, focally dilated intrahepatic ducts due to multifocal strictures (arrows), consistent with sclerosing cholangitis (TurboRARE with respiratory gating (TR 150) and partial Fourier transform acceleration factor 1.3, echo time 8 ms, effective echo time 16, RARE factor 4, image matrix $512 \times 256 \times 256$ pixels, acquisition matrix $394 \times 168 \times 198$ pixels, resolution 100 μm isotropic, acquisition time 25 min with respiratory rate of $\sim$25 breaths/min).

Table 2 Ability to detect biliary tree features in mdr2 knockout, bile duct-ligated, and control mice

	microCT	MR
mdr2 knockout mice		
Gallbladder	+	+
Extrahepatic bile ducts	+/−	+
Intrahepatic bile ducts	−	+
Cholelithiasis	−	+
Ductal strictures	−	+/−
Ductal dilation	−	+
Ductal irregularity	−	+
Bile duct ligation mice		
Gallbladder	NA	+
Extrahepatic bile ducts	NA	+
Intrahepatic bile ducts	NA	+
Gallbladder dilation	NA	+
Ductal dilation	NA	+
Wild-type (control) mice		
Gallbladder	NA	+
Extrahepatic bile ducts	NA	+
Intrahepatic bile ducts	NA	+/−

microCT, micro-computerized tomography; MR, nuclear magnetic resonance imaging (any method); NA, not assessed.
−, 0% of mice; +/−, infrequently or inconsistently; +, consistently (>75% of mice).

shorten scanning times (depending on the objectives of the particular experiment, and weighing the potential physiologic impact and risks of repeated contrast injection for longitudinal studies). We believe that as with the clinical MRCP experience, development of a murine MR cholangiography protocol will require further work guided in part by the above, as well as the experience of other investigators. Until then, a combination of multiple methods is likely to provide the most comprehensive information, but fewer methods can be used depending on the question of interest.

In conclusion, noninvasive mouse MR cholangiography is a feasible and promising method for assessment and longitudinal monitoring of hepatobiliary disease *in vivo*. Our findings thus far encourage further development and optimization of this method, as well as adaptation to a broader range of mouse and other small rodent models of cholangiopathy.

Supplementary Information accompanies the paper on the Laboratory Investigation website (http://www.laboratoryinvestigation.org)

DISCLOSURE/CONFLICT OF INTEREST

The authors declare no conflict of interest.

1. Lazaridis KN, Strazzabosco M, Larusso NF. The cholangiopathies: disorders of biliary epithelia. Gastroenterology 2004;127:1565–1577.
2. Tabibian JH, Masyuk AI, Masyuk TV, LaRusso NF. Cholangiocyte Physiology. Comprehensive Physiology 2013;3:541–565.
3. Tabibian JH, O'Hara SP, Larusso NF. Primary sclerosing cholangitis: the gut-liver axis. Clin Gastroenterol Hepatol 2012;10:819.
4. Lindor KD. Ursodiol for primary sclerosing cholangitis. Mayo Primary Sclerosing Cholangitis-Ursodeoxycholic Acid Study Group. N Engl J Med 1997;336:691–695.
5. O'Hara SP, Tabibian JH, Splinter PL, *et al*. The dynamic biliary epithelia: molecules, pathways, and disease. J Hepatol 2012;58:575–582.
6. Boonstra K, Beuers U, Ponsioen CY. Epidemiology of primary sclerosing cholangitis and primary biliary cirrhosis: a systematic review. J Hepatol 2012;56:1181–1188.
7. Bambha K, Kim WR, Talwalkar J, *et al*. Incidence, clinical spectrum, and outcomes of primary sclerosing cholangitis in a United States community. Gastroenterology 2003;125:1364–1369.
8. Fickert P, Zollner G, Fuchsbichler A, *et al*. Ursodeoxycholic acid aggravates bile infarcts in bile duct-ligated and Mdr2 knockout mice via disruption of cholangioles. Gastroenterology 2002;123:1238–1251.
9. Pollheimer MJ, Trauner M, Fickert P. Will we ever model PSC? – ''it's hard to be a PSC model!''. Clin Res Hepatol Gastroenterol 2011;35: 792–804.
10. Tabibian JH, Lindor KD. Primary sclerosing cholangitis: a review and update on therapeutic developments. Expert Rev Gastroenterol Hepatol 2013;7:103–114.
11. Tabibian JH, Weeding E, Jorgensen RA, *et al*. Randomised clinical trial: vancomycin or metronidazole in patients with primary sclerosing cholangitis - a pilot study. Aliment Pharmacol Ther 2013;37:604–612.
12. Wiesner RH, LaRusso NF. Clinicopathologic features of the syndrome of primary sclerosing cholangitis. Gastroenterology 1980;79:200–206.
13. Vitellas KM, Keogan MT, Freed KS, *et al*. Radiologic manifestations of sclerosing cholangitis with emphasis on MR cholangiopancreatography. Radiographics 2000;20:959–975.
14. Chapman R, Fevery J, Kalloo A, *et al*. Diagnosis and management of primary sclerosing cholangitis. Hepatology 2010;51:660–678.
15. Fickert P, Fuchsbichler A, Wagner M, *et al*. Regurgitation of bile acids from leaky bile ducts causes sclerosing cholangitis in Mdr2 (Abcb4) knockout mice. Gastroenterology 2004;127:261–274.
16. Wallner BK, Schumacher KA, Weidenmaier W, *et al*. Dilated biliary tract: evaluation with MR cholangiography with a T2-weighted contrast-enhanced fast sequence. Radiology 1991;181:805–808.
17. Dave M, Elmunzer BJ, Dwamena BA, *et al*. Primary sclerosing cholangitis: meta-analysis of diagnostic performance of MR cholangiopancreatography. Radiology 2010;256:387–396.
18. Tabibian JH, Lindor KD. Challenges of cholangiocarcinoma detection in patients with primary sclerosing cholangitis. J Analyt Oncol 2012;1:5.
19. Hirao K, Miyazaki A, Fujimoto T, *et al*. Evaluation of aberrant bile ducts before laparoscopic cholecystectomy: helical CT cholangiography versus MR cholangiography. Am J Roentgenol 2000;175: 713–720.
20. Fleischmann D, Ringl H, Schofl R, *et al*. Three-dimensional spiral CT cholangiography in patients with suspected obstructive biliary disease: comparison with endoscopic retrograde cholangiography. Radiology 1996;198:861–868.
21. Yeh BM, Breiman RS, Taouli B, *et al*. Biliary tract depiction in living potential liver donors: comparison of conventional MR, mangafodipir trisodium-enhanced excretory MR, and multi-detector row CT cholangiography–initial experience. Radiology 2004;230:645–651.
22. Alvaro D, Alpini G, Onori P, *et al*. Effect of ovariectomy on the proliferative capacity of intrahepatic rat cholangiocytes. Gastroenterology 2002;123:336–344.
23. Reagan-Shaw S, Nihal M, Ahmad N. Dose translation from animal to human studies revisited. FASEB J 2008;22:659–661.
24. Dalal PU, Howlett DC, Sallomi DF, *et al*. Does intravenous glucagon improve common bile duct visualisation during magnetic resonance cholangiopancreatography? Results in 42 patients. Eur J Radiol 2004;49:258–261.
25. Gong AY, Masyuk AI, Splinter PL, *et al*. Channel-mediated water movement across enclosed or perfused mouse intrahepatic bile duct units. Am J Physiol Cell Physiol 2002;283:C338–C346.
26. Tabibian JH, Asham EH, Han S, *et al*. Endoscopic treatment of postorthotopic liver transplantation anastomotic biliary strictures with maximal stent therapy (with video). Gastrointest Endosc 2010;71:505–512.
27. Witczak-Malinowska K, Gorycki T, Stalke P, *et al*. Value of magnetic resonance cholangiography (MRC) in primary sclerosing cholangitis (PSC). Med Sci Monit 2001;7(Suppl 1):114–117.
28. MacCarty RL, LaRusso NF, Wiesner RH, *et al*. Primary sclerosing cholangitis: findings on cholangiography and pancreatography. Radiology 1983;149:39–44.
29. van Nieuwerk CM, Groen AK, Ottenhoff R, *et al*. The role of bile salt composition in liver pathology of mdr2 (-/-) mice: differences between males and females. J Hepatol 1997;26:138–145.
30. Masyuk TV, Radtke BN, Stroope AJ, *et al*. Inhibition of Cdc25A suppresses hepato-renal cystogenesis in rodent models of polycystic kidney and liver disease. Gastroenterology 2012;142:622–633.e4.
31. O'Hara SP, Splinter PL, Trussoni CE, *et al*. Cholangiocyte N-Ras protein mediates lipopolysaccharide-induced interleukin 6 secretion and proliferation. J Biol Chem 2011;286:30352–30360.
32. Vierling JM, Hreha G, Wang H, *et al*. The role of biliary epithelial cells in the immunopathogenesis of non-suppurative destructive cholangitis in murine hepatic graft-versus-host disease. Trans Am Clin Climatol Assoc 2011;122:326–335.
33. Figueiredo JL, Siegel C, Nahrendorf M, *et al*. Intraoperative near-infrared fluorescent cholangiography (NIRFC) in mouse models of bile duct injury. World J Surg 2010;34:336–343.
34. Sparks EE, Huppert KA, Brown MA, *et al*. Notch signaling regulates formation of the three-dimensional architecture of intrahepatic bile ducts in mice. Hepatology 2010;51:1391–1400.
35. Masyuk TV, Ritman EL, LaRusso NF. Quantitative assessment of the rat intrahepatic biliary system by three-dimensional reconstruction. Am J Pathol 2001;158:2079–2088.
36. Zhang X, Yang XR, Chen Y, *et al*. Diffraction-enhanced radiography of various mouse organs. Am J Roentgenol 2010;195:545–549.